American Mineralogist, Volume 92, pages 1158–1164, 2007

P-V and *T-V* Equations of State of natural biotite: An in-situ high-pressure and high-temperature powder diffraction study, combined with Mössbauer spectroscopy

A. Pavese,[1,2,*] N. Curetti,[3] V. Diella,[2] D. Levy,[3] M. Dapiaggi,[1] and U. Russo[4]

[1]Dipartimento Scienze della Terra, Università degli Studi di Milano, Via Botticelli 23- 20133 Milano, Italy
[2]National Research Council, IDPA, Section of Milan, Via Botticelli 23-20133 Milano, Italy
[3]Dipartimento di Scienze Mineralogiche e Petrologiche, Università degli Studi di Torino, Via Valperga Caluso 37-10125 Torino, Italy
[4]Dipartimento di Scienze Chimiche, Università di Padova, Via Marzolo 1-35131 Padova, Italy

Abstract

The *P-V* and *T-V* equations of state of a natural biotite sample (Mg/Fe ratio ≈ 1) have been studied using in-situ high-pressure (0.0001–11 GPa) synchrotron radiation powder diffraction at the European Synchrotron Radiation Facilities (ESRF) in Grenoble, France, and in-situ high-temperature (298–610 K) laboratory X-ray powder diffraction. A third-order Birch-Murnaghan model [V_0 = 498.7(1) Å^3, measured value] provides the following elastic parameters: K_0 = 49(1) GPa, K' = 8.1(5). The volume thermal expansion is satisfactorily described by a constant value resulting in 37(2) 10^{-6} K^{-1}. Mössbauer spectroscopy proves that REDOX reactions have occurred upon heating, presumably $2(OH^- + Fe^{2+}) \rightarrow 2O^{2-} + 2Fe^{3+} + H_2^{\uparrow}$ and/or $4Fe^{2+} + 2OH^- + O_2 \rightarrow 4Fe^{3+} + 3O^{2-} + H_2O$. On the basis of the elastic and thermal parameters measured we have modeled the deformation contribution (G_{deform}) to the Gibbs energy. The third-order Birch-Murnaghan model with V_0 fixed at its experimental value and the model with refined V_0 do not significantly differ from one another in terms of G_{deform}. A comparison based on G_{deform} between biotite and phlogopite shows a better compliance to P of the former, though balanced in mineral reactions by a difference of molar volume, i.e., V_0(biotite) > V_0(phlogopite).

Keywords: High-pressure studies, high-temperature studies, biotite, *P-T* stability

Introduction

Biotites [ideally $K(Fe,Mg,Al,Ti)_3(AlSi_3)O_{10}(OH)_2$] are widespread micas, involved in many petrogenetic reactions occurring in a variety of natural environments ranging from igneous to metamorphic (Proyer 2003; Puziewicz and Johannes 1988; Icenhower and London 1995; Palmieri et al. 2003). Such solid solutions play a relevant role in fluid-absent melting processes, as reviewed by Vielzeuf and Schmidt (2001), and in mineral-fluid interactions, as discussed by Zeng et al. (1990). Biotites are able to provide storage of H_2O in the lithosphere, in relation to deformed and metamorphosed rocks (Nakashima et al. 1995). In particular, the assemblage biotite-orthopyroxene-Kfeldspar-quartz is adopted to estimate H_2O in magmatic and high-grade metamorphic rocks (Graphchikov et al. 1999). A general review of the role of biotites as geothermobarometers can be found in Fleet (2003). In the last twenty years, the study of petrogenetic processes has largely benefited from modeling and numerical simulations (Holland and Powell 1998), which have accrued their importance as a support to experimental activities both for interpretation and prediction (Wei and Powell 2004). The knowledge of calorimetric (see Ogorodova et al. 2005a, 2005b, for the case of biotite) and thermo-elastic parameters of minerals has grown crucial to allow a reliable modeling of stability and transformations of mineral phases or assemblages at high pressure and temperature conditions. In such a view, the investigation of the biotite behavior in terms of elastic parameters (bulk modulus and its first-second derivatives vs. pressure) and volume thermal expansion is important to properly account for the contribution of this mica to a multitude of reactions (Hermann 2001; Hermann and Green 2001). Note that the compositions of biotites result from complex atomic replacements involving cations and hydroxyl group (Busigny et al. 2004; Abrecht and Hewitt 1988); for this reason, comparative studies on elastic and thermal properties of biotites are a key to set a solid basis (1) on one hand to the understanding of the effects due to atomic substitutions in trioctahedral micas, and (2) on the other hand to the development of a flexible modeling which is able to fit a variety of petrological environments.

Relatively few experimental studies aimed at enhancing insights into elastic and thermal properties of micas have been carried out to date (see for a review Zanazzi and Pavese 2002); such a paucity is apparent in the case of biotites [see the high-temperature neutron powder diffraction study of Chon et al. (2003)]. This is presumably due to the difficulties in finding appropriate single crystals free of the many defects commonly affecting the biotite structure (Toshihiro and Banfield 2000;

* E-mail: alessandro.pavese@unimi.it

Toshihiro and Nespolo 2001). Recently, Comodi et al. (2004) and Pavese et al. (2003a) have undertaken investigations on the behavior of phlogopite at high-pressure conditions. A study of the properties of biotite at non-ambient conditions may therefore represent a complement to those quoted above.

In this work we report data on the pressure-volume (*P-V*) Equation of State (EoS) and temperature-volume (*T-V*) EoS of a natural biotite sample, with a composition characterized by (1) a Fe/Mg ratio close to unity, and (2) a relatively low ^{VI}Ti-^{VI}Al content. In-situ high-pressure (HP) powder diffraction measurements have been performed at ESRF, while high-temperature (HT) experiments have been carried out by means of a laboratory powder diffractometer, equipped with a furnace. Different *P-V* EoS models and the way in which they affect the field of stability of biotite are presented. The measured elastic properties of biotite are compared with those of phlogopite, and the relative behavior under compression is discussed in terms of deformation energy.

Experimental methods

Sample

The natural biotite used has been sampled from a quartz-diorite rock of the central body of the pluton of Val Biandino, Lecco (Italy). Quantitative chemical analyses were performed on polished sample using an Applied Research Laboratories electron microprobe fitted with six wavelength-dispersive spectrometers and a Tracor Northern Energy Dispersive Spectrometer. The system was operated using an accelerating voltage of 15 kV, a sample current on brass of 15 nA and a counting time of 20 s on the peaks and 10 s on the backgrounds. Natural minerals (kaersutite for Si, Mg, Na,Ti, K, Fe, Al, and rodonite for Mn) were employed as standards. The results were processed for matrix effects using a conventional ZAF routine in the Tracor Northern TASK series of programs. The chemical composition, determined by averaging 22 analysis points and assuming OH only, results in:

$$[K_{0.92(1)}Na_{0.01(3)}]_{\Sigma 0.93}[Mg_{1.31(6)}Fe_{1.35(1)}Al_{0.06(1)}Ti_{0.18(3)}]_{\Sigma 2.90}[Al_{1.15(2)}Si_{2.85(3)}]_{\Sigma 4}O_{10}(OH)_2$$

where normalization is based on 11 O atoms. Between parentheses are reported the corresponding e.s.d. values. Crystallinity, phase composition and symmetry of the sample in question have been preliminarily tested using an 'XPERT Philips diffractometer. Chlorite, which occurs in modest amount (<5–7% in weight), has been partially removed by a manual picking. The symmetry of the biotite sample is consistent with 1M-polytype (space group *C*2/*m*). The quality of crystallinity has proven sufficient for a reliable lattice parameter determination; grain size ≤10 μm.

The cell parameters determined by synchrotron radiation X-ray diffraction at room conditions are: a = 5.3441(2), b = 9.2571(6), c = 10.246(1) Å, β = 100.31(3)°, and V = 498.7(1) Å^3, the latter to be compared to 495.6(3) Å^3 of Bigi and Brigatti (1994).

High-pressure powder diffraction

High-pressure powder diffraction experiments have been performed at the ID9A beamline of ESRF (Grenoble, F), adopting an angle dispersive set-up. A Pt-coated vertical-focalizing mirror and a cut bent Si(111) horizontal-focusing Laue monochromator focus the beam from an undulator source into a spot size at the sample ≈30 × 30 μm^2 and λ = 0.4172 Å, the latter determined by a NIST-Si calibration. HP conditions have been achieved by means of a diamond anvil cell with 600 μm culets, hole size ≈200 μm diameter, using N_2 as a pressure-transmitting medium. The *P*-values have been measured by the fluorescence line shift of ruby, excited by an Ar-laser and adopting the non-linear pressure scale of Mao et al. (1986). Equilibrium at a given pressure has been assumed when *P*-oscillations do not exceed 0.02–3 GPa, monitored every tenth minute. A nominal uncertainty of 0.1 GPa has been used based on our previous studies carried out with the same experimental set-up (Curetti et al. 2006). Non-hydrostaticity of *P* is a problem commonly affecting these kinds of experiments. Levy et al. (2003), using the same experimental HP set-up, devised an a-posteriori correction of *P*, but observed that it does not affect significantly the elastic parameters measured. Therefore, we have chosen to use the raw *P*-values. Two data collections have been performed to improve our observation statistics. Diffraction signals have been recorded by a MAR345 imaging plate with 100 μm resolution placed at 365.54 mm from the sample, so as to provide a 0.04° angular resolution; exposure time was shorter than 1 min, read-out and erasing within 8–9 min. 2-D diffraction images were first been cleared of the signals from solid N_2, and subsequently turned into 1-D intensity-2θ patterns (FIT2D program; Hammersley et al. 1996), suited to standard Rietveld/Le Bail profile treatments. The HP powder diffraction patterns have been modeled [GSAS software package (Larson and Von Dreele 2000)] by Pseudo-Voigt profile functions, parametrizing their Gaussian and Lorentzian FWHM components as $\sigma^2 = \sigma_0^2$ and $\gamma = Y_0/\cos(\theta)$, where σ_0 and Y_0 are the refinable coefficients . Background and preferred orientation have been described by Chebyshev polynomials and March-Dollase model (Dollase 1986), respectively. Figure 1 shows experimental and calculated diffraction patterns at 10 GPa.

High-temperature powder diffraction

High-temperature Cu-wavelength X-ray powder diffraction measurements have been carried out by a laboratory diffractometer (Philips 'XPERT), equipped with a furnace (AHT PAP-1600). A stepper motor shifts the sample downward as a function of the sample holder thermal expansion, to provide an optimal sample position throughout the *T*-range explored. Reliable data collections may be obtained even above 1600 K, taking into account that 1900 K is the upper heating limit of the furnace. Si-NBS (640c) has been used as an internal calibrant for an accurate evaluation of the goniometer zero correction. Data collections were performed at 298, 352, 404, 463, 524, 557, 608, and 668 K, between 5 and 110 °2θ, with a step size of 0.02 °2θ, a counting time of 5 s per step, and a heating rate of 25 °/min. The temperature on the sample is provided by the calibration discussed by Dapiaggi et al. (2002), assuming an uncertainty of about ±2 K. The sample was continuously flushed with He during heating to limit possible oxidation processes. The GSAS package (Larson and Von Dreele 2000) was used to treat our HT powder diffraction data, adopting the Pseudo-Voigt profile function to model the experimental patterns. The Gaussian and Lorentzian FWHM components were parameterized as $\sigma^2 = \sigma_0^2$ and $\gamma = Y_0/\cos(\theta) + X_0 \tan(\theta)$, respectively, and σ_0^2, Y_0, X_0 refined. The goniometer zero, determined at room temperature, was fixed in the HT diffraction pattern treatments; the absence of any sample displacement aberration was verified by checking the peak positions of the internal standard at each temperature.

Mössbauer spectroscopy

Room-temperature Mössbauer spectroscopy measurements have been performed on the biotite sample before and after heating to investigate whether REDOX reactions have occurred. The sample was prepared as follows: (1) fine grinding of about 20 mg of biotite in an agate mortar under acetone; (2) preparation of a suspension in vaseline; (3) insertion of the suspension into a lead container and subsequent wrapping in a thin plastic foil. A conventional constant acceleration spectrometer and a rhodium matrix ^{57}Co source (nominal strength 50 mCi) have been used in the present measurements. Mirror symmetric spectra have been recorded by a 512-channel analyzer, folded and fitted by Lorentzian-like profile functions; no thickness correction has been required, because of the amount of material used. A "magic angle" setting has been adopted to reduce the effects due

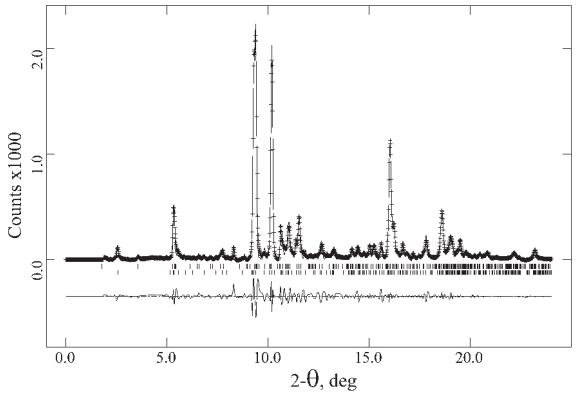

Figure 1. High-pressure observed, calculated, and residual (obs-calc) powder diffraction patterns at 10 GPa of biotite. Peak positions are marked by vertical bars.

to preferred orientation, which are common in micas. Figure 2 displays the spectra collected on the biotite sample before and after heating.

Results and discussion

P-V EoS

In Table 1, the lattice parameters as a function of pressure are presented. The results from the Birch-Murnaghan EoS (Birch 1986) fit to the *P-V* data are reported in Table 2. Figure 3 shows the V/V_0-P curve in the case of the third-order Birch-Murnaghan EoS, with V_0 fixed (BM3 model). In Figure 4, the normalized pressure, defined as $P_{normalized} = P/[3f_E(1 + 2f_E)^{5/2}]$ is plotted as a function of the Eulerian strain (f_E); an inflection seems to take place between 0.02 and 0.03 value of f_E. We attribute this to the uncertainties, presumably larger than those reported, in determining both lattice parameters and pressure, which may cause scatter of points. $P_{normalized}$ as a function of f_E exhibits an overall linearity, though some values lie outside of the trend, suggesting that a third-order Birch model be sufficient to fit the present data. The refinement of V_0 in the third-order Birch-Murnaghan EoS (BM3V) does not provide a significant improvement in terms of χ^2 and produces K_0 and K' shifts within 3σ with respect to the corresponding values obtained with V_0 fixed. However, the K_0-K' plot, here not shown for the sake of brevity, reveals that BM3 and BM3V may in principle be envisaged as two distinct models, the latter lying slightly outside of the 99% confidence ellipse centered on the former. The cases of the fourth-order Birch-Murnaghan EoS with V_0 not refined (BM4) and V_0 refined (BM4V) are shown in Table 2, for comparison only. In fact, though BM4 and BM4V yield remarkably smaller χ^2 values than BM3 and BM3V, the elastic properties obtained by the fourth-order truncation are not physically meaningful. In particular, $K' < 1\sigma$ and $K'' \approx 3\sigma$, implying that K'' is more significant than K', which is in apparent contradiction to the hypothesis of convergence of the coefficients of a phenomenological EoS-expansion, such as the Birch-Murnaghan model.

Had we used the Vinet model, we would have obtained K_0 = 49(1) GPa and K' = 7.9(4), and K_0 = 45(2) GPa, K' = 8.6(6), and V_0 = 500.0(9) Å^3, in full accordance with the third-order Birch EoS. Altogether, BM3 is the model which best combines (1) a reasonably small number of parameters (K_0 and K') and (2) a satisfactory observed-calculated agreement; for these reasons we elect it as a reference in the following discussion.

The values of BM3 are compared with those provided by Comodi et al. (2004) and Pavese et al. (2003a), who report for phlogopite [K_0 = 54(2) GPa; K' = 7(1); V_0 = 497.1(1) Å^3] and [K_0

Table 1. Pressure and lattice parameters of biotite

P (GPa)	*a* (Å)	*b* (Å)	*c* (Å)	β (°)	*V* (Å^3)
0	5.3441(2)	9.2571(6)	10.246(1)	100.31(3)	498.7(1)
0.4(1)	5.3387(2)	9.2501(4)	10.183(2)	100.50(1)	494.4(1)
0.8(1)	5.3317(2)	9.2340(4)	10.124(1)	99.587(9)	491.47(6)
1.5(1)	5.3283(5)	9.2114(5)	10.054(2)	99.90(1)	486.1(1)
1.9(1)	5.3235(3)	9.2034(3)	10.027(1)	100.64(1)	482.82(6)
2.2(1)	5.3182(3)	9.1967(5)	10.020(1)	100.63(1)	481.64(6)
3.1(1)	5.3031(3)	9.1756(6)	9.913(1)	100.58(1)	474.16(6)
3.9(1)	5.2922(3)	9.1543(5)	9.861(1)	100.62(1)	469.55(6)
4.5(1)	5.2816(3)	9.1359(4)	9.806(1)	100.60(1)	465.08(6)
5.4(1)	5.2693(4)	9.1173(6)	9.727(2)	100.76(1)	459.1(1)
6.0(1)	5.2677(2)	9.1069(4)	9.705(1)	100.74(1)	457.41(6)
6.1(1)	5.2629(3)	9.1019(5)	9.703(1)	100.68(1)	456.73(6)
6.8(1)	5.2535(4)	9.0822(5)	9.651(1)	100.48(1)	452.78(7)
7.0(1)	5.2535(3)	9.0836(4)	9.641(1)	100.81(1)	451.91(6)
7.2(1)	5.2474(6)	9.077(1)	9.639(1)	100.69(1)	451.14(9)
7.6(1)	5.2457(2)	9.0703(4)	9.622(1)	100.84(1)	449.65(6)
8.1(1)	5.2400(3)	9.0566(5)	9.588(2)	100.92(1)	446.8(1)
8.6(1)	5.2338(3)	9.0457(6)	9.569(2)	100.90(1)	444.9(1)
8.7(1)	5.225(1)	9.043(2)	9.543(1)	100.29(2)	443.7(1)
9.1(1)	5.2270(3)	9.0404(5)	9.554(1)	100.91(1)	443.30(6)
10.0(1)	5.2207(3)	9.0239(4)	9.510(1)	100.95(1)	439.87(6)
10.3(1)	5.2098(2)	9.0203(4)	9.4961(8)	100.09(1)	439.35(5)
11.4(1)	5.1951(2)	9.0066(4)	9.4380(5)	100.13(1)	434.72(4)
11.9(1)	5.1933(5)	9.0049(8)	9.4308(7)	100.19(1)	434.07(7)

Table 2. Elastic parameters determined by the Birch-Murnaghan model

Model	K_0(GPa)	K'	K'' (GPa^{-1})	V_0 (Å^3)	χ^2
BM3	49(1)	8.1(5)	–0.5047	498.6829	1.9
BM3V	45(3)	9.1(7)	–0.7727	500.0(9)	1.8
BM4	59(3)	0.6(2)	1.4(4)	498.6829	1.1
BM4V	62(4)	–0.4(22)	1.4(6)	498.2(6)	1.1

Notes: $\chi^2 = 1/(N - M)\Sigma_j(P_{obsj} - P_{EoSj})^2/\sigma^2$, where N is the number of pressure points, M the degrees of freedom, P_{obs} = observed pressure; P_{EoS} = pressure calculated by EoS. $\sigma^2 = [\sigma(P)^2 + (\partial P/\partial V)^2\sigma(V)^2]$.

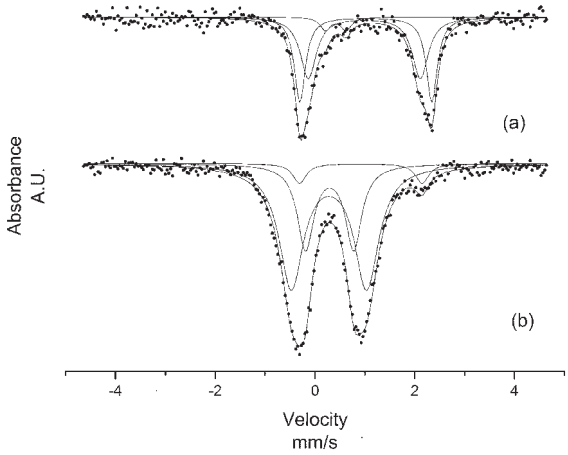

Figure 2. Mössbauer patterns of biotite before (**a**) and after (**b**) heating. Lines correspond to modeling and solid circles to experimental data.

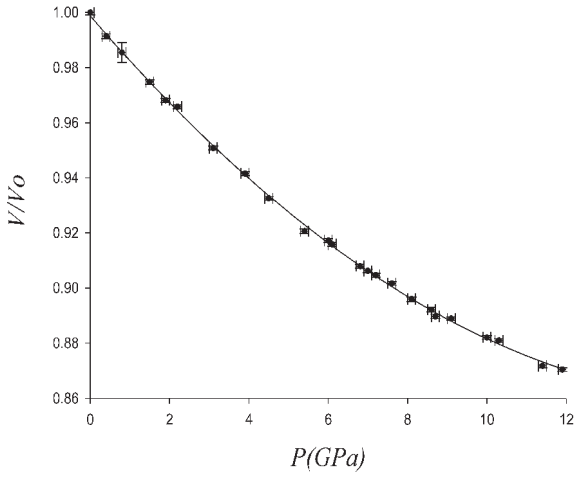

Figure 3. V/V_0 of biotite as a function of pressure. Solid circles = observations; solid line = fit by the BM3 model.

= 49.7(5) GPa; K' = 8.6(2); V_0 = 488.6(2) Å^3], respectively. K_0 and K' values of biotite deviate from those of phlogopite within 3σ. The above authors determined K_0-values of phlogopite larger than that reported here for biotite; in the case of K' Comodi et al. (2004) give K'(phlogopite) < K'(biotite), whereas Pavese et al. (2003) claim K'(phlogopite) > K'(biotite). Therefore, one concludes that (1) the elastic parameters of biotite are very similar to those of phlogopite; and (2) the main difference involves K'. The discrepancies in the molar volumes between phlogopite samples are accounted for by Tombolini et al. (2002), who pointed out that V_0 in phlogopite micas changes significantly as a function of the Fe-content, ranging from 487.5 Å^3 in the case of a Mg-rich composition, to 500 Å^3 in ferroan-phlogopite specimens.

Axial compressibilities of biotite have been determined by fitting a third-order Birch-Murnaghan EoS to P values using a^3, b^3, and c^3 instead of V. In so doing, one attains: β_a = 0.00252(6), β_b = 0.0035(1), and β_c = 0.0143(5) GPa^{-1}, at ambient conditions. Such values indicate that about 13%, 17%, and 70% bulk compressibility distributes along [100], [010], and [001], respectively. In the case of phlogopite, Comodi et al. (2004) provide a relative compression partitioned as 15%, 14%, 71%, whereas Pavese et al. (2003a) indicate 13%, 14%, 73%. All this leads one to conclude that biotite responds anisotropically to P, as does phlogopite. In both micas the volume shrinkage occurs principally at the expense of the c-axis (~70%). The a and b cell parameters show similar shortening rates.

T-V EoS

The lattice parameters and the volume of biotite as a function of T are displayed in Figures 5 and 6, respectively, and reported in Table 3. The large uncertainties of a and b are related to the Bragg-Brentano collection geometry that enhances the (00l)-harmonics because of the preferred orientation promoted by the quasi-ideal cleavage of micas. One observes that the trends exhibited by a, b, and c are linear within the experimental uncertainties, save the point at the highest T for which b and c abruptly drop. We are inclined to attribute this behavior to a possible dehydroxylation/deprotonation reaction, which occurs in combination with a Fe-oxidation at high temperature [see Fleet (2003) for a review]. The latter has been confirmed by Mössbauer spectroscopy, which will be discussed in the ensuing section. The regularity shown by the trends of the unit-cell parameters up to ≈610 K makes us confident that the 298–610 K data can be used for the determination of the thermal expansion coefficient; oxidation processes are assumed either to have not

TABLE 3. Lattice parameters of biotite as a function of temperature

T (K)	a (Å)	b (Å)	c (Å)	β (°)	V (Å^3)
298	5.3441(2)	9.2571(6)	10.246(1)	100.31(3)	498.7(1)
352	5.3447(31)	9.2605(37)	10.2556(12)	100.35(1)	499.3(8)
404	5.3481(37)	9.2660(31)	10.2650(11)	100.32(1)	500.5(8)
463	5.3505(32)	9.2744(30)	10.2784(14)	100.39(1)	501.7(6)
524	5.3553(40)	9.2846(36)	10.2901(13)	100.38(1)	503.3(6)
557	5.3581(40)	9.2932(30)	10.2965(13)	100.21(1)	504.6(6)
608	5.3613(40)	9.2970(30)	10.3127(17)	100.34(1)	505.7(7)
668	5.3639(70)	9.2583(70)	10.3058(14)	99.78(1)	504.4(8)

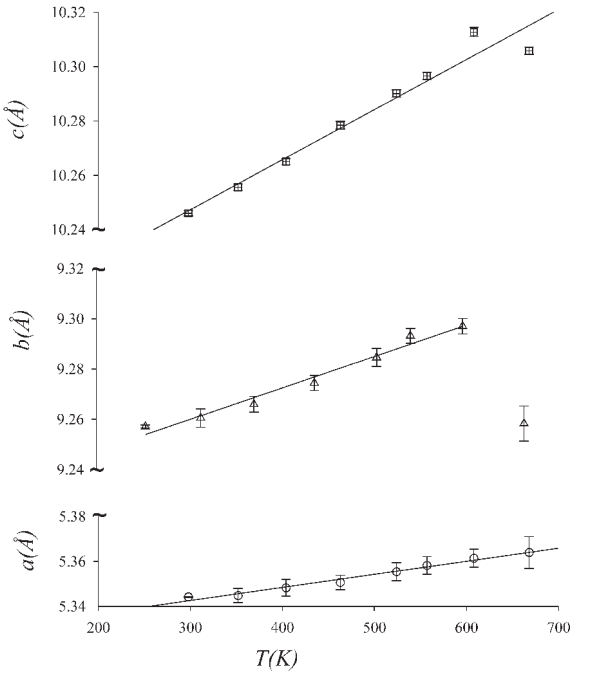

FIGURE 5. Lattice parameters of biotite as a function of temperature.

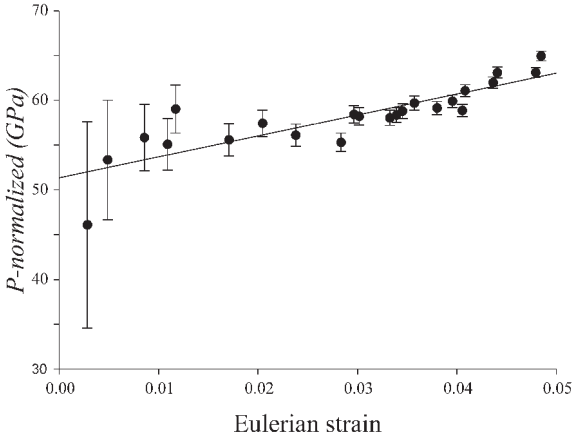

FIGURE 4. Normalized pressures ($P_{normalized}$) as a function of Eulerian strain, f_E.

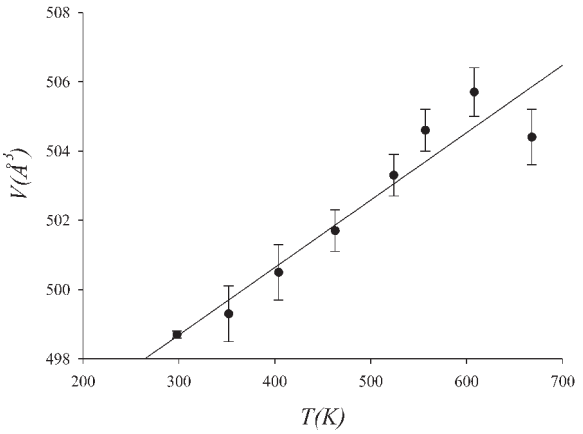

FIGURE 6. Volume of biotite as a function of temperature.

yet started, or to be reasonably negligible at $T < 610$ K. These results fully agree with those of an in-situ HT neutron powder diffraction study by Chon et al. (2003). Tutti et al. (2000) claim that Fe-oxidation in phlogopite occurs over the 773–873 K range, which also supports the hypothesis that our biotite sample is unaffected by oxidation up to 610 K. A linear function of T, $C + A(T - T_0)$, has been used to fit $\ln(l/l_0)$, where l is a generic lattice parameter, or the cell volume; as a consequence, the thermal expansion function of l reduces to the A constant. If one uses $C + A(T - T_0) + B(T - T_0)^2$ to model $\ln(l/l_0)$, one attains a second-order coefficient as large as $\approx 2\sigma$. Hence, a linear polynomial in T yields: $\alpha_a = 10.9(7)\ 10^{-6}$, $\alpha_b = 15.0(9)\ 10^{-6}$, $\alpha_c = 20.4(6)\ 10^{-6}$, $\alpha_V = 37(2)\ 10^{-6}\ K^{-1}$. Anisotropy is revealed in the (001) plane by a comparison between α_a and α_b. Tutti et al. (2000) also observe anisotropy in (001) in phlogopite, but measure $\alpha_a > \alpha_b$, whereas Russell and Guggenheim (1999) report $\alpha_a \approx \alpha_b$. Chon et al. (2003) determine in a natural biotite α_a, α_b, α_c as large as 4.4, 5.2, and 16.5 $10^{-6}\ K^{-1}$, respectively; these values are smaller than ours and smaller than those generally reported in literature for trioctahedral micas (Zanazzi and Pavese 2002).

Mössbauer spectroscopy results

Table 4 shows the results obtained by Mössbauer spectroscopy measurements carried out before and after heating. Prior to heating the Fe^{3+} content in natural biotite is 6–7 wt% with respect to total Fe; after thermal treatment, the Fe^{3+} content increases to 95–96 wt%. The Mössbauer pattern of biotite before heating shows the presence of an asymmetric doublet attributable to Fe^{2+}, and a shoulder around 0 mm/s due to a small amount of Fe^{3+}. The spectrum of the heated sample exhibits a broad doublet centered at low velocity, fitted by two Fe^{3+} components, and a small peak at high velocity ($\approx$2 mm/s) produced by Fe^{2+}. According to the quadruple splitting values it is possible to assign an octahedral coordination to all the sites occupied by iron in both samples, though the ΔE_Q values hint to different site distortions or/and second coordination spheres (Cesare et al. 2005; Pavese et al. 2003b). Accurate IR-spectroscopic measurements might help to interpret the transformation at ~670 K, but would not add information relevant to the purpose of the present work. We hypothesize two possible oxidization reactions, which might account for a change from ferrous to ferric iron, and for a decomposition of the hydroxyl group:

$$2(OH^- + Fe^{2+}) \rightarrow 2O^{2-} + 2Fe^{3+} + H_2^{\uparrow}$$

corresponding to the deprotonation process proposed by Pavese et al. (2003b), and

TABLE 4. Results by room temperature Mössbauer spectroscopy on biotite sample before and after heating

Sample	β* mm/s	βEQ mm/s	Γ mm/s	A %	Attribution
biotite before	1.13(1)	2.64(1)	0.26(2)	46(2)	Octahedral Fe(II)
heating	1.10(1)	2.24(2)	0.38(3)	48(2)	Octahedral Fe(II)
	0.52(4)	0.41(8)	0.25(6)	7(3)	Octahedral Fe(III)
biotite after	1.03(2)	2.45(5)	0.32(6)	6(3)	Octahedral Fe(II)
heating	0.39(3)	1.51(3)	0.59(2)	65(2)	Octahedral Fe(III)
	0.40(3)	0.96(2)	0.40(4)	30(2)	Octahedral Fe(III)

* Relative to room temperature β-Fe foil.

$$4Fe^{2+} + 2OH^- + O_2 \rightarrow 4Fe^{3+} + 3O^{2-} + H_2O$$

wherein a dehydroxylation takes place jointly with a REDOX reaction involving iron and atmospheric oxygen. Both reactions do not necessarily imply a change of coordination of iron; the latter, in particular, might provide an additional interstitial oxygen.

Stability of biotite under compression

We explore now (1) how the different *P-V* EoS models developed here, in particular BM3 and BM3V, affect the *P*-stability of biotite, and (2) how the *P-T* stability of biotite may be related to the stability of phlogopite. Our analysis is focused on the deformation contribution (G_{deform}) to the Gibbs energy, i.e., that part of energy accounting for pure compression and dependent on the thermoelastic parameters discussed in the present work. G_{deform} is calculated from the integral

$$G_{deform} = \int_{0,T}^{P,T} V(P',T)\, dP'$$

where (P,T) and $(0,T)$ fix the extremes of integration along a T-isotherm from ambient pressure (approximated by 0) to a given pressure P. G_{deform} gives therefore a measure of the "tendency" of a phase to stabilize under pressure , at a given temperature, and is the key for modeling HP processes. Note that $dG_{deform}/dP = G'_{deform} = V(P,T)$. Figure 7 shows $\Delta G_{deform} = G(BM3)_{deform} - G(BM3V)_{deform}$ as a function of P at room temperature, illustrating the G_{deform}-differences between BM3 and BM3V. For the sake of comparison, the configuration entropy of a fully disordered cation distribution over the octahedral sites of our biotite sample amounts to $\approx$1.8 kJ/mol per 100 K shift, thus providing a significantly larger contribution than ΔG_{deform}. This suggests that BM3 and BM3V do not yield significantly different G_{deform}-values, with respect to the other components to the total Gibbs energy; the quoted models only begin to show significant differences in the very high pressure regime above 20 GPa, where even small changes of K_0-K'-V_0 may produce non-negligible energetic contributions. In Figure 8, $G'(\text{phlogopite})_{deform}/G'(\text{biotite})_{deform}$, i.e., $V(\text{phlogopite})/V(\text{biotite})$, is displayed as a function of pressure, using the elastic parameters of phlogopite from Pavese et al.(2003a), derived from a sample whose composition is close to that of ideal phlogopite.

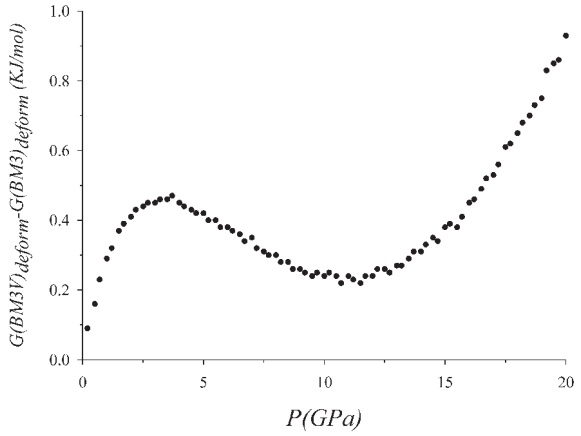

FIGURE 7. Deformation energy difference as a function of P, between BM3V and BM3 models.

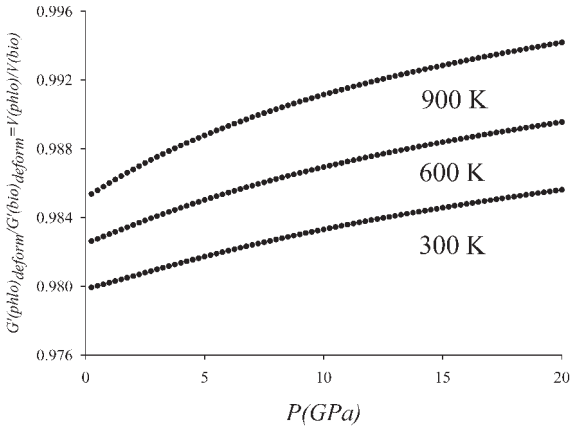

FIGURE 8. $G'(\text{phlogopite})_{\text{deform}}/G'(\text{biotite})_{\text{deform}} = V(\text{phlogopite})/V(\text{biotite})$, as a function of P and T.

The P-V-T relationship in our calculations has been modeled by the third-order Birch P-V EoS extended to high temperature, as discussed by Pavese (2002); dK/dT from Pavese et al. (1999), α_V of phlogopite from Comodi et al. (2004). The predicted positive slope of $G'(\text{phlogopite})_{\text{deform}}/G'(\text{biotite})_{\text{deform}}$ proves that $G(\text{phlogopite})_{\text{deform}}$ increases "more rapidly" than $G(\text{biotite})_{\text{deform}}$ under pressure. This can be accounted for by the relationships $K_0(\text{phlogopite}) > K_0(\text{biotite})$ and $K'(\text{phlogopite}) > K'(\text{biotite})$, which imply a more effective compliance to P in the case of biotite. The curve $G(\text{phlogopite})_{\text{deform}}/G(\text{biotite})_{\text{deform}}$ not shown here for brevity, exhibits a decreasing trend with pressure, substantiating the above conclusion. In principle, this means that biotite has a tendency to become more stable with increasing P, in terms of pure deformation energy, than phlogopite. However, this behavior is balanced in reactions by the absolute G_{deform}-values of the micas in question. Based on the molar volumes, [$V_0(\text{biotite}) > V_0(\text{phlogopite})$], $G(\text{biotite})_{\text{deform}} > G(\text{phlogopite})_{\text{deform}}$, which is consistent with the observed stability of phlogopite at HP. This latter statement may be appreciated by considering the fictitious reaction, "phlogopite – 1.5MgO(periclase) + 1.5FeO(wüstite) = biotite," which gives, by way of example, $G(\text{biotite})_{\text{deform}} - G(\text{phlogopite} - 1.5\ \text{periclase} + 1.5\ \text{wüstite})_{\text{deform}} \approx 6.5$ kJ/mol, at 4 GPa-300 K [G_{deform} for sole biotite and phlogopite: 580 and 569 kJ/mol, respectively], and ≈11.9 kJ/mol, at 8 GPa-300 K [G_{deform} for sole biotite and phlogopite: 1131 and 1110 kJ/mol, respectively] (thermo-elastic data for MgO and FeO from Ahrens 1995).

ACKNOWLEDGMENTS

The European Synchrotron Radiation Facility is kindly acknowledged for allocating beam time to carry out HP measurements and Italian National Research Council—CNR, Istituto per la dinamica dei processi ambientali, section of Milan—for microanalysis facilities. The authors are grateful to Hans-Peter Liermann and an anonymous referee for useful comments, suggestions, and corrections.

REFERENCES CITED

Abrecht, J. and Hewitt, D.A. (1988) Experimental evidence on the substitution of Ti in biotite. American Mineralogist, 73, 1275–1284.

Ahrens, T.J. (1995) Mineral physics and crystallography: a handbook of physical constants. AGU Reference Shelf 2.

Bigi, S. and Brigatti, M.F. (1994) Crystal chemistry and microstructures of plutonic biotite. American Mineralogist, 79, 63–72.

Birch, F. (1986) Equation of state and thermodynamic parameters of NaCl to 300 kbar in the high temperature domain. Journal Geophysical Research, 83, 1257–1268.

Busigny, V., Cartigny, P., Philippot, P., and Javoy, M. (2004) Quantitative analysis of ammonium in biotite using infrared spectroscopy. American Mineralogist, 89, 1625–1630.

Cesare, B., Meli, S., Nodali, L., and Russo, U. (2005) Fe^{3+} reduction during biotite melting in graphitic metapelites: another origin of CO_2 in granulites. Contributions to Mineralogy and Petrology, 149, 129–140.

Chon, C.M., Kim Shi, A., and Moon Hi, S. (2003) Crystal structures of biotite at high temperatures and heat-treated biotite using neutron powder diffraction. Clays and Clay Minerals, 51, 519–528.

Comodi, P., Fumagalli, P., Montagnoli, M., and Zanazzi, P.F. (2004) A single crystal study on the pressure behavior of phlogopite and petrological implications. American Mineralogist, 89, 647–653.

Curetti, N., Levy, D., Pavese, A. and Ivaldi, G. (2006) Elastic properties and stability of coexisting 3T and 2M_1 phengite polytypes. Physics and Chemistry of Minerals, 32, 670-678

Dapiaggi, M., Artioli, G., and Petras, L. (2002) A newly developed high-temperature chamber for in-situ X-ray diffraction: setup and calibration procedures. The Rigaku Journal, 19, 35–41.

Dollase, W.A. (1986) Correction of intensities for preferred orientation in powder diffractometry: application of the March model. Journal of Applied Crystallography, 19, 267–272.

Fleet, M.E. (2003) Rock-forming Minerals. Sheet silicates: Micas. Volume 3A, second edition. The Geological Society, London.

Graphchikov, A.A., Konilov, A.N., and Clemens, J.D. (1999) Biotite dehydration, partial melting and fluid composition; experiments in the system $KAlO_2$-FeO-MgO-SiO_2-H_2O-CO_2. American Mineralogist, 84, 15–26.

Hammersley, A.P., Svensson, S.O., Hanfland, M., Fitch, A.N., and Häusermann, D. (1996) Two-dimensional detector software: from real detector to idealised image or two-theta scan. High Pressure Research, 14, 235–248.

Hermann, J. (2001) Experimental constraints on phase relations in subducted continental crust. Contributions to Mineralogy and Petrology, 143(2), 219–235.

Hermann, J. and Green, D.H. (2001) Experimental constraints on high pressure melting in subducted crust. Earth and Planetary Science Letters, 188, 149–168.

Holland, T.J.B. and Powell, R. (1998) An internally consistent data set for phases of petrological interest. Journal of Metamorphic Geology, 16, 309–343.

Icenhower, J. and London, D. (1995) An experimental study of element partitioning among biotite, muscovite and coexisting peraluminous silicic melt at 200 MPa (H_2O). American Mineralogist, 80, 1229–1251.

Larson, A.C. and Von Dreele, R.B. (2000) General Structure Analysis System (GSAS). Los Alamos National Laboratory Report LAUR 86-748.

Levy, D., Pavese, A., and Hanfland, M. (2003) Synthetic $MgAl_2O_4$(spinel) at high pressure conditions (0.0001–30 GPa): A X-ray powder diffraction by synchrotron radiation. American Mineralogist, 88, 93–98.

Mao, H.K., Xu, J., and Bell, P.M. (1986) Calibration of the ruby pressure gauge to 800 kbar under quasi-hydrostatic conditions. Journal of Geophysical Research, 91, 4673–4676.

Nakashima, S., Matayoshi, H., Yuko, T., Michibayashi, K., Masuda, T., Kuroki, N., Yamagishi, H., Ito, Y., and Nakamura, A. (1995) Infrared microspectroscopy analysis of water distribution in deformed and metamorphosed rocks. Tectonophysics, 245, 263–276.

Ogorodova, L.P., Kiseleva, I.A., and Mel'chakova, L.V. (2005a) Thermodynamic properties of biotite. Russian Journal of Physical Chemistry, 79, 1387–1389.

Ogorodova, L.P., Kiseleva, I.A., Mel'chakova, L.V., and Shuriga, T.N. (2005b) High-temperature heat capacity of biotites. Geochemistry International, 43, 804–806 (translated from Geokhimiya, 8, 886–888, 2005).

Palmieri, R., Ghiribelli, B., and Ricci, C.A. (2003) Ultra-high-pressure metamorphism in felsic rocks; the garnet-phengite gneiss and quartzites from Lanterman Range, Antartica. European Journal of Mineralogy, 15, 513–525.

Pavese, A. (2002) Pressure volume temperature equations of state: a comparative study based on numerical simulations. Physics and Chemistry of Minerals, 29, 43–51.

Pavese, A., Ferraris, G., Pischedda, V., and Mezouar, M. (1999) Synchrotron powder diffraction study of phengite 3T from the Dora-Maira massif: P-V-T equation of state and petrological consequences. Physics and Chemistry of Minerals, 26, 460–467.

Pavese, A., Levy, D., Curetti, N., Diella, V., Fumagalli, P., and Sani, A. (2003a) Equation of state and compressibility of pholgopite by in situ high pressure X-ray powder diffraction experiments. European Journal of Mineralogy, 15, 455–463.

Pavese, A., Curetti, N., Ferraris, G., Ivaldi, G., Russo, U., and Ibberson, R. (2003b) Deprotonation and order-disorder reactions as a function of temperature in a phengite 3T (Cima Pal, western Aps) by neutron diffraction and Mössbauer spectroscopy. European Journal of Mineralogy, 15, 357–363.

Proyer, A. (2003) Metamorphism of pelites in NKFMASH—a new petrogenetic grid with implications for the preservation of high-pressure mineral assemblages

during exhumation. Journal of Metamorphic Geology, 21, 493–509.
Puziewicz, J. and Johannes, W. (1988) Phase equilibria and compositions of iron-magnesium-aluminum minerals and melts in water-saturated peraluminous granitic systems. Contributions to Mineralogy and Petrology, 100, 156–168.
Russell, R.L. and Guggenheim, S. (1999) Crystal structures of near-end-member phlogopite at high temperature and heat treated Fe-rich phlogopite: the influence of the O,OH,F site. Canadian Mineralogist, 37, 711–720.
Tombolini, F., Brigatti, M.F., Marcelli, A., Cibin, G., Mottana, A., and Giuli, G. (2002) Local and average Fe distribution in trioctahedral micas: Analysis of Fe *K*-edge XANES spectra in the phlogopite–annite and phlogopite–tetraferriphlogopite joins on the basis of single-crystal XRD refinements. European Journal of Mineralogy, 14, 1075–1085.
Toshihiro, K. and Banfield, J.F. (2000) New insights into the mechanism of chloritization of biotite using polytype analysis. American Mineralogist, 85, 1202–1208.
Toshihiro, K. and Nespolo, M. (2001) Atomic structures of planar defects in oxybiotite. American Mineralogist, 86, 336–340.
Tutti, F., Dubrovinsky, L.S., and Nygren, M. (2000) High-temperature study and thermal expansion of phlogopite. Physics and Chemistry of Minerals, 27, 599–603.
Vielzeuf, D. and Schmidt, M.W. (2001) Melting relations in hydrous systems revisited: application to metapelites, metagreywackes and metabasalts. Contributions to Mineralogy and Petrology, 141, 251–267.
Wei, C. and Powell, R. (2004) Calculated phase relations in high-pressure metapelites in the system NKFMASH (Na_2O-KO_2-FeO-MgO-Al_2O_3-SiO_2-H_2O). Journal of Petrology, 45, 183–202.
Zanazzi, P.F. and Pavese, A. (2002) Behavior of micas at high pressure and high temperature conditions. In A. Mottana, F.P. Sassi, J.B. Thompson, and S. Guggenheim, Eds., Micas: Crystal Chemistry and Metamorphic Petrology, 46, p. 499. Reviews in Mineralogy and Geochemistry, Mineralogical Society of America, Chantilly, Virginia.
Zeng, Y., Feng, Z., and Hao, J. (1990) Interaction between biotite and Na-Ca-chloride fluid at 500 °C and 1 kbar. Neues Jahrbuch für Mineralogie Monatshefte, 11, 517–520.

Manuscript received June 22, 2006
Manuscript accepted February 19, 2007
Manuscript handled by Przemyslaw Dera